Sensors and Actuators B 250 (2017) 574–583

Contents lists available at ScienceDirect

Sensors and Actuators B: Chemical

journal homepage: www.elsevier.com/locate/snb

Micropatterning of metal oxide nanofibers by electrohydrodynamic (EHD) printing towards highly integrated and multiplexed gas sensor applications

Kyungnam Kang[a,b,c], Daejong Yang[a,b,c,d], Jaeho Park[a,b,c], Sanghyeok Kim[a,b,c], Incheol Cho[a,b,c], Hyun-Ho Yang[e], Minkyu Cho[a,b,c], Saeb Mousavi[a,b,c], Kyung Hyun Choi[f,**], Inkyu Park[a,b,c,*]

[a] Department of Mechanical Engineering, KAIST, Daejeon 34141, Republic of Korea
[b] KI for the NanoCentury, KAIST, Daejeon 34141, Republic of Korea
[c] Mobile Sensor and IT Convergence (MOSAIC) Center, KAIST, Daejeon 34141, Republic of Korea
[d] Department of Medical Engineering, California Institute of Technology, Pasadena, CA 91125, United States
[e] Department of Electrical and Computer Engineering, University of California at San Diego, La Jolla, CA 92093, United States
[f] Department of Mechatronics Engineering, Jeju National University, Jeju 690-756, Republic of Korea

ARTICLE INFO

Article history:
Received 5 March 2017
Received in revised form 26 April 2017
Accepted 28 April 2017
Available online 1 May 2017

Keywords:
Metal oxide nanofiber
Chemiresistive gas sensor
Gas sensor array
MEMS
Electrohydrodynamic (EHD) printing
Electrospinning

ABSTRACT

Integration of heterogeneous sensing materials in microelectronic devices is essential to accomplish compact and highly integrated environmental sensors. For this purpose, a micro-patterning method of electrospun metal oxide nanofibers based on electrohydrodynamic (EHD) printing process was developed in this work. Several types of metal oxide (SnO_2, In_2O_3, WO_3 and NiO) nanofibers that were produced by electrospinning, fragmented into smaller pieces by ultrasonication, and dissolved in organic solvents were utilized as inks for the printing. Constant or pulsed wave bias consisting of base and jetting voltages were applied between a nozzle and a substrate to generate a jetting of nanofiber solutions. Several parameters for EHD printing such as pulse width, inner diameter of the nozzle, distance from the nozzle to the substrate, and stage speed, were optimized for accurate micro-patterning of electrospun nanofibers. By using optimized printing parameters, microscale patterns of electrospun nanofibers with a minimum diameter less than 50 μm could be realized. Gas sensors were fabricated by EHD printing on the microelectrodes and then used for the detection of toxic gases such as NO_2, CO and H_2S. Four kinds of metal oxides could detect down to 0.1 ppm of NO_2, 1 ppm of H_2S and 20 ppm of CO gases. Also, heterogeneous nanofiber gas sensor array was fabricated by the same printing method and could detect NO_2 using the sensor array platform with microheaters. Furthermore, microscale patterns of nanofibers by EHD printing could be applied to the suspended MEMS platform without any structural damage and this sensor array could detect NO_2 and H_2S gases with 20 mW power consumption.

1. Introduction

Recently, the importance of personalized air quality monitoring is increasing due to the rising interests in the personal health issues related to the air pollution. Although conventional air monitoring systems utilizing optical sensing, mass spectroscopy and gas chromatography have good accuracy, they are not appropriate for personalized air quality monitoring due to high prices and poor portability. For the personalized gas sensing, catalytic combustion [1], electrochemical [2,3], field effect transistor [4–6] and chemiresistive type [7–11] gas sensors have been commonly utilized. Among them, chemiresistive type sensor is the most appropriate for portable and personalized gas sensing due to its simple operation principle, high sensitivity, versatility to various target gases, low prices and possibility of miniaturization [12]. Various sensing materials such as graphene, carbon nanotubes (CNTs), silicon, polymer and metal oxide nanomaterials have been employed for the chemiresistive type gas sensors [5,8–10,13–18].

Metal oxide gas sensor can detect various gases using the chemical reaction at the surfaces and sensing data can be simply obtained

* Corresponding author at: Department of Mechanical Engineering, KAIST, Daejeon 34141, Republic of Korea.
** Corresponding author.
E-mail addresses: khchoi@jejunu.ac.kr (K.H. Choi), inkyu@kaist.ac.kr (I. Park).

http://dx.doi.org/10.1016/j.snb.2017.04.194
0925-4005/

by measuring the electrical resistance of the sensing material. However, metal oxide nanomaterial based gas sensors generally suffer from low selectivity [19]. In order to resolve this problem, various techniques have been developed such as optimization of operating temperatures, doping catalysts on the sensing materials or usage of molecular filters [20–23]. Another useful approach is to employ an array of different metal oxide materials, which can provide specific combination of sensing responses to certain single-component gas or mixed gases [21] and improve the accuracy of target gas identification via signal processing techniques such as principal component analysis (PCA).

Until now, drop casting, screen printing, inkjet printing, etc. have been utilized to deposit metal oxide nanomaterials on the gas sensor arrays [24–27]. However, these processes have several limitations for the fabrication of highly integrated and miniaturized gas sensor array. For example, screen printing requires a printing mask for the fabrication of the sensor array and consumes large volume of materials, but it only provides limited printing resolution (minimum size ~100 μm). Drop casting method also cannot provide fine patterning due to the large droplet size as well as the spreading of the deposited solution. Inkjet printing can directly fabricate microscale patterns on the substrate without any mask or photoresist patterning, but it is difficult to print high viscosity solutions with a high density of sensing materials and clogging problem occurs with smaller nozzles used for fine patterning [28,29].

In this paper, electrohydrodynamic (EHD) printing of metal oxide nanomaterials has been used as an alternative to the abovementioned methods for the fabrication of highly integrated and miniaturized gas sensor array. The EHD printing can produce patterns smaller than the inner diameter of the nozzle [28] and can even print high viscosity solutions, which is not possible by the inkjet printing method [28,29]. This is due to the mechanism of EHD printing based on the pulling of solution by an intense electric field between the needle and the substrate [30]. Until now, EHD printing has been widely utilized to generate microscale patterns of metal nanoparticles [31], polymer [30,32], etc. To the best of our knowledge, the usage of EHD printing for metal oxide nanofiber patterning has not been reported before. In this work, electrospun metal oxide nanofibers were used as sensing materials because they are known to have very high sensitivity due to their high surface areas and porosities [33,34]. By fragmentation of electrospun nanofibers into shorter pieces (length of a few micrometers) and using their solution for EHD printing with optimal process parameters, sub–50 μm patterns that are smaller than the diameter of the nozzle can be easily fabricated. By EHD printing of various metal oxide nanofibers in series or in parallel, a highly integrated sensor array of heterogeneous metal oxide nanofibers can be easily manufactured (see Fig. 1). In this study, we utilized this method to implement a gas sensor array of three kinds of electrospun nanofibers (SnO_2, WO_3 and In_2O_3) on the suspended MEMS platform that can detect an oxidizing gas (NO_2) as well as reducing gases (H_2S) with high sensitivity and low power consumption (20 mW per each MEMS microheater).

2. Material and methods

2.1. Electrospinning of metal oxide nanofibers and their fragmentation

Four types of metal oxide nanofibers (SnO_2, WO_3, In_2O_3 and NiO) were synthesized by electrospinning process. For SnO_2 nanofibers, PVAc (Polyvinyl acetate, Mw: 500,000) as a template polymer, tin (IV) acetate as a metal source and acetic acid were mixed with N,N-dimethlyformamide as a solvent [35,36]. This solution was stirred with a magnetic bar at room temperature for 2 h. The precursor solution was loaded to a 5 mL plastic syringe with a 25G metal needle connected to a high voltage supply. A bias of 16 kV was applied to the metal needle that was separated from the aluminum foil by a distance of 15 cm while the flow rate of solution was fixed at 20 μL/min. Long nanofibers were formed on the aluminum foil by the electrospinning process with high electric field. After the formation of polymer-metal complex nanofibers, the electrospun nanofibers casted on the substrate were sintered at 500 °C for 30 mins in order to remove the binding polymer and to crystalize the metal oxide [35,36]. For WO_3, In_2O_3 and NiO nanofibers, abovementioned process was repeated with different source materials and synthesis parameters as summarized in Table S1 (Supplementary Information).

The electrospun nanofibers should be fragmented to smaller pieces in order to form printable solutions in the EHD printing process. Each metal oxide was mixed with ethanol, and ultrasonication process was conducted for an hour in order to break the nanofibers into shorter pieces. After the ultrasonication, the ethanol in the nanofiber solution was evaporated in a convection oven at 70 °C for 9 h. The dried electrsopun fibers were finally dispersed in alpha-terpineol or ethyleneglycol solvents with 15 wt% concentration.

2.2. EHD printing of nanofiber fragments: micropatterning (line and dot arrays)

The ink solution made by ultrasonication of elecrospun nanofibers was loaded in the syringe of the EHD printing system. A function generator (Agilent 33210A) and a high voltage amplifier (TREK 10/10B-HS) were used to generate electrical pulses. A syringe and a pump system were used to eject the precursor solution. Dual cameras were used to monitor the ejection process and to align the syringe needle with the printing substrate. A solution of metal oxide nanofibers in alpha-terpineol or ethyleneglycol (15 wt%) was loaded to the syringe with a needle tip of 90 μm inner diameter. Various metal oxide nanofiber patterns were printed on a $Au/SiO_2/Si$ substrate. For line patterns, a constant DC bias of 1.3 kV–1.5 kV was applied to the needle while the distance between the needle tip and the substrate was fixed at 200 μm. The pattern shapes were controlled using a programmable X-Y stage motion controller at a speed of 1 mm/s. Dot patterns were also printed on the substrate by applying pulse wave bias consisting of a base voltage (1.0–1.3 kV) and a jetting voltage (1.2–1.5 kV). The width of the pulse wave was changed from 100 ms to 500 ms and 1 s. The frequency of the pulse wave was fixed at 0.2 Hz (Fig. S1 in the Supplementary Information).

2.3. Fabrication of sensor platform

Gold sensing electrodes were fabricated on a SiO_2 (2 μm thickness by thermal oxidation)/Si substrate for the gas sensing platform that operates in a tube furnace. In order to pattern the gold electrodes, AZ5214 photoresist (PR) was first coated on the SiO_2/Si substrate by using a spin coater. Then, interdigitated electrodes arrays were patterned by standard UV photolithography. A Cr/Au (10 nm/200 nm) layer was deposited on the PR-patterned wafer using an electron beam (e-beam) evaporator followed by lift-off. For a sensor array platform integrated with microheaters, Cr/Pt (10 nm/200 nm) microheater electrodes were fabricated via e-beam evaporation on a SiO_2/Si substrate followed by the deposition of 600 nm thick SiO_2 layer via plasma enhanced chemical vapor deposition (PECVD) for electrical insulation. On top of the SiO_2 insulation layer, Cr/Au (10 nm/200 nm) interdigitated sensing electrodes were fabricated by e-beam evaporation. Finally, Pt heater pads were opened for the electrical contact by selective etching of SiO_2 insulation layer with buffered oxide etchant (BOE).

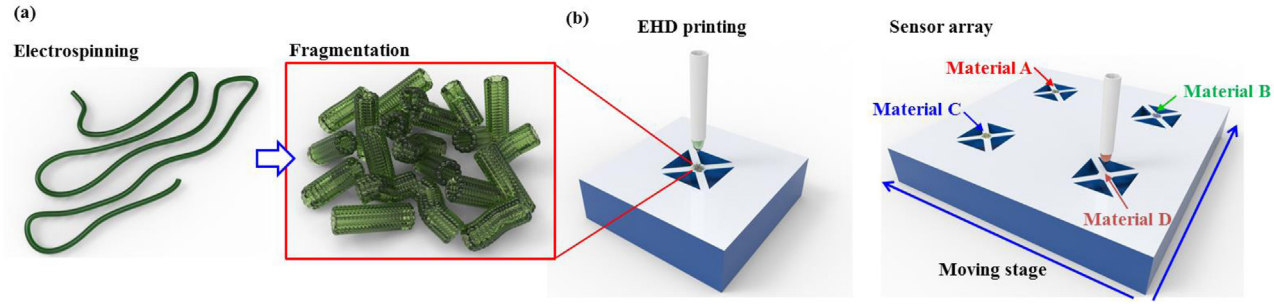

Fig. 1. Fabrication of highly integrated gas sensor array by EHD printing of electrospun nanofibers: (a) metal oxide nanofiber fragments are prepared by electrospinning and fragmentation process (e.g. ultrasonication); (b) highly integrated gas sensor array is fabricated by micro-patterning of heterogeneous metal oxide nanofibers via sequential or parallel EHD printing process.

For the low-power suspended MEMS platform, SiO_2 layer (1 μm) was deposited by PECVD process on the pure Si wafer and subsequent processes for electrode, insulation layer and microheater that are the same as those for the abovementioned non-suspended microheater devices were conducted. In order to eliminate the residual stress of SiO_2 film, annealing process was carried out at 350 °C for 1 h in N_2 atmosphere. Finally, XeF_2 or tetramethylammonium hydroxide (TMAH) etching were carried out for the formation of suspended microheater. We confirmed that the bending of suspended microheater due to the residual stress was negligible by optical microscopy. Furthermore, we verified an outstanding thermomechanical stability of suspended microheater through an accelerated static heating (at 30 mW; i.e. 50% higher heating power than operational heating condition (20 mW) of the sensor) and a cyclic pulsed heating tests (rectangular heating pulse with 5 s on (22 mW) + 5 s off (0 mW) for over 24 h).

2.4. EHD printing of electrospun nanofibers with accurate alignment on the microelectrode

A syringe needle and a printing substrate were aligned using dual cameras and a X-Y stage for the printing of metal oxide nanofibers on the sensing electrode. A pulse wave with 100 ms of pulse width was used for the printing of nanofiber fragments. After the initial EHD jetting, the pulse wave produced by a function generator and high voltage amplifier was turned off to produce a single jet pattern.

2.5. I–V characteristics

In order to measure the electrical characteristics of micropatterns of various metal oxide nanofiber fragments, bias sweep from −5 V to 5 V was applied across the sensing electrodes, and the current through the metal oxide nanofiber network was measured using a semiconductor analyzer (Hewlett-Packard 4155A).

2.6. Gas test with NO_2, CO and H_2S gases (tube furnace or microheater)

Gas detection tests for NO_2, CO and H_2S gases were conducted using the EHD printed metal oxide gas sensors, which were installed in a tube furnace set at specific temperatures (300 °C or 450 °C). Various concentrations of each gas were injected into the tube furnace using mass flow controllers. In order to measure the resistance change of the metal oxide nanofiber network, a constant bias (3.0 V) was applied across the sensing electrode while the current was measured using a source meter (Keithley 2400, 2636B). In case of sensor array with microheaters, sensing materials were heated by microheaters instead of using a tube furnace. For the sensor array bounded on the Si substrate, a voltage of 4.5 V was applied across the microheater. On the other hand, for the MEMS sensor array suspended from the Si substrate, a voltage of 2.0–2.4 V was applied across microheater. A bias of 3.0 V was commonly applied to the sensing electrode to measure the current through the sensing material during the exposure to target gas.

3. Results and discussions

By using the electrospinning process explained above, various metal oxide nanofibers (SnO_2, WO_3, In_2O_3 and NiO) were synthesized as shown in Fig. 2. Because of the calcination process after the electrospinning, the polymers used as nanofiber templates were decomposed to synthesize these metal oxide nanofibers from tin (IV) acetate, ammonium metatungstate hydrate, indium nitrate hydrate and nickel nitrate hexahydrate, respectively. Fig. 2 presents SEM images of various metal oxides and corresponding energy dispersive spectrometer (EDS) data verifying the elemental compositions of each metal oxide nanofiber. Small carbon peaks observed in all EDS spectra might be originated from incomplete decompositions of the polymers after sintering process. All electrospun nanofibers formed web-like network, in which each nanofiber was longer than several micrometers. The average diameters of nanofibers measured from the SEM images were 320 nm for SnO_2, 230 nm for WO_3, 97 nm for In_2O_3, and 60 nm for NiO. SnO_2 nanofibers were in tubular shapes with very thin walls and WO_3 nanofibers exhibited the shape with myriads of cylindrical nanorods. In_2O_3 nanofibers showed very smooth and straight geometry with no observable particles on the surface. On the other hand, NiO nanofibers showed granular microstructure with a rough surface.

Fig. 3 shows the line patterns of SnO_2 nanofibers using the EHD printing with a constant DC bias (1.3 and 1.5 kV). The DC bias from the function generator was amplified by one thousand times using a high voltage amplifier. The electric field of 65 MV/m between the nozzle and the substrate resulted in the electrostatic force to pull the solution from the nozzle to the substrate. To understand the electric field distributions in the EHD system when a bias is applied, a numerical simulation was performed using COMSOL Multiphysics® software as shown in Fig. S2 (Supplementary Information). Due to the equal potential on both sidewalls of the steel nozzle, electric field comes from the inner wall to center of nozzle and heads for the substrate ground. Because of the electric field from the nozzle to the substrate, the liquid solution undergoes an electrostatic force and is pulled out from the nozzle. When a liquid meniscus is formed at the end of the nozzle, the forces exerted to the meniscus reach an equilibrium that can be described by the following equation:

$$\sigma_s + \sigma_h + \sigma_e = 0$$

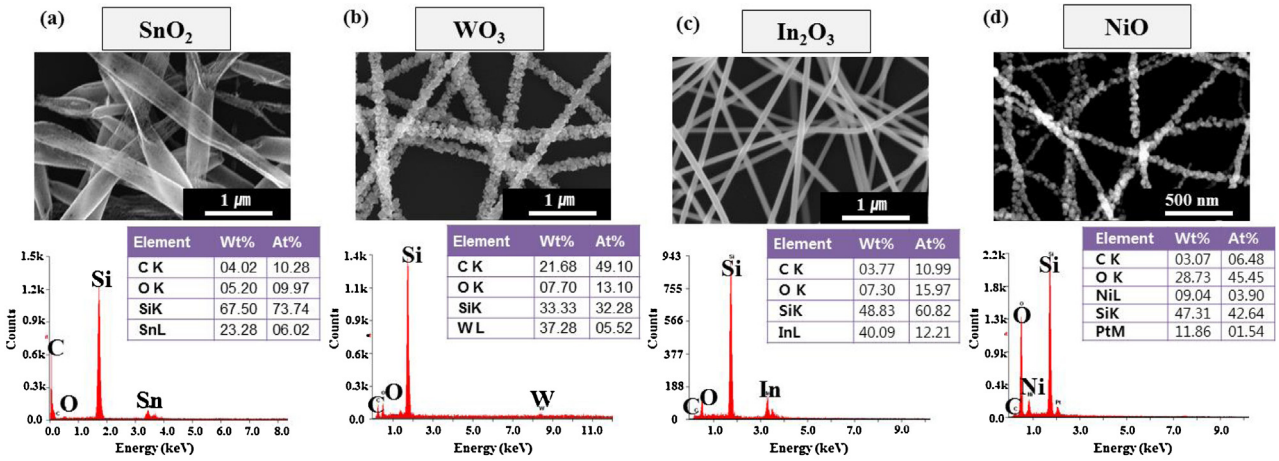

Fig. 2. SEM images and EDS spectra of (a) SnO_2, (b) WO_3, (c) In_2O_3, (d) NiO electrospun nanofibers. After calcination process, most of polymer templates were thermally decomposed and metal oxide nanofibers were formed.

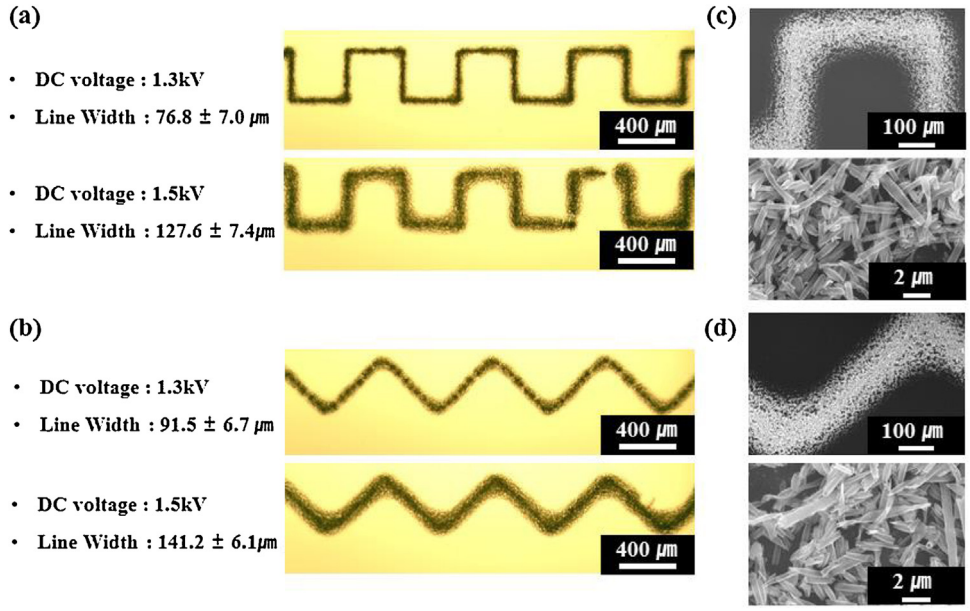

Fig. 3. Optical microscope images of EHD line patterns in (a) square and (b) triangular wave shapes by applying different DC bias, and SEM images of each pattern (c) and (d). These lines were composed of nanofiber fragments. By increasing the input bias, line width was increased due to higher electric field and larger amount of ejected nanofibers.

where σ_s is the surface tension, σ_h is the hydrostatic pressure, and σ_e is the electrostatic pressure [37].

When a nominal bias is applied between the nozzle and the substrate, the mobile ions of the solution in the nozzle are accumulated near the surface of the meniscus. The mobile ions in the solution repulse each other due to the Coulombic force, and the summation of the Coulombic force as a whole becomes a tangential force on the surface of the meniscus, resulting in a cone shape meniscus. In the case that sufficiently high electric field is applied between the nozzle and the substrate, σ_e becomes greater than the summation of σ_s and σ_h, and then droplets can be ejected from the apex to drive out the accumulated surface charge [30]. Fig. S3 (Supplementary Information) verifies this explanation. Below 1.1 kV, the ionized solution is simply moved to the end of nozzle and a spherical meniscus is formed. As the applied voltage is increased to 1.1 kV, the spherical meniscus is changed to a cone shape because the increased electric field causes more ions to accumulate toward the substrate. At a bias of 1.2 kV, the droplet is ejected from the apex by the breakage of the equilibrium among σ_s, σ_h and σ_e.

With sufficiently high DC bias, a jetting of solution occurs continuously until the bias is turned off, so that continuous line patterns are formed on the $Au/SiO_2/Si$ substrate. Because the X-Y motion stage can be programmed in moving trajectories, square and triangular wave line patterns could be easily fabricated by using EHD printing with X-Y motion stage control. In our EHD printing system, continuous jetting occurred when 1.3 kV bias was applied to the nozzle. As increasing the applied bias to 1.5 kV, more solution was pulled out from the nozzle due to higher electric field, and therefore the line width was increased (Square wave line: width = 76.8 ± 7.0 μm at 1.3 kV → width = 127.6 ± 7.4 μm at 1.5 kV, Triangular wave line: width = 91.5 ± 6.7 μm at 1.3 kV → width = 141.2 ± 6.1 μm at 1.5 kV). In the high resolution SEM images (Fig. 3(c) and (d)), we could observe that the line patterns were composed of a few micrometer long flakes of electrospun nanofibers that were fragmented using the ultrasonication process before the EHD printing. The printing results in Fig. S4 (Supplementary Information) show discontinuous line patterns of electrospun nanofibers at lower bias (1.2 kV).

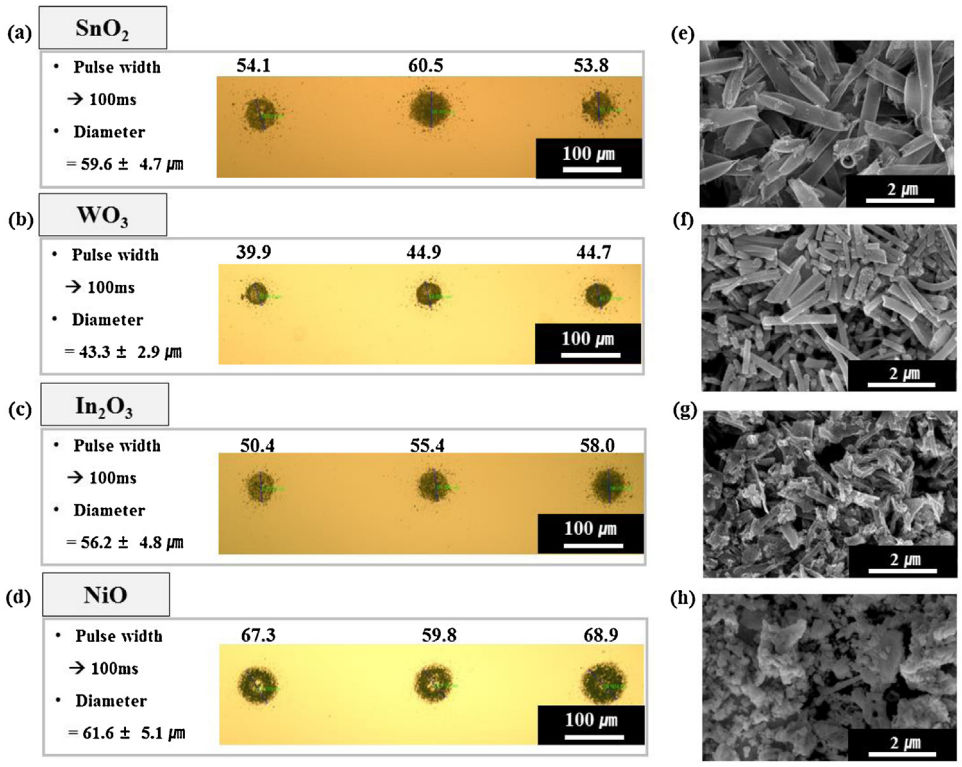

Fig. 4. EHD printing results of (a) SnO_2, (b) WO_3, (c) In_2O_3 and (d) NiO nanofibers on gold electrodes with 100 ms pulse width. SEM images of EHD printed solution in each pattern: (e) SnO_2, (f) WO_3, (g) In_2O_3 and (h) NiO nanofibers. Single dot pattern consists of nanofiber fragments and patterns show diameters in the range of 40–70 μm.

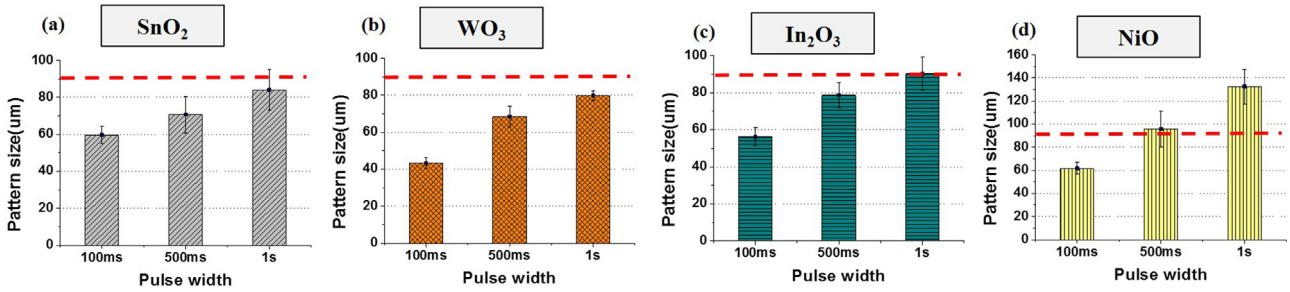

Fig. 5. Average pattern sizes of various EHD-printed metal oxide patterns depending on the pulse width: (a) SnO_2, (b) WO_3, (c) In_2O_3 and (d) NiO nanofibers. Pattern size was proportional to pulse width (100 ms, 500 ms and 1 s). Longer pulse width increased the volume of solution jetting, resulting in bigger patterns. The red dashed lines indicate the inner diameter of the nozzle, 90 μm. (For interpretation of the references to colour in this figure legend, the reader is referred to the web version of this article.)

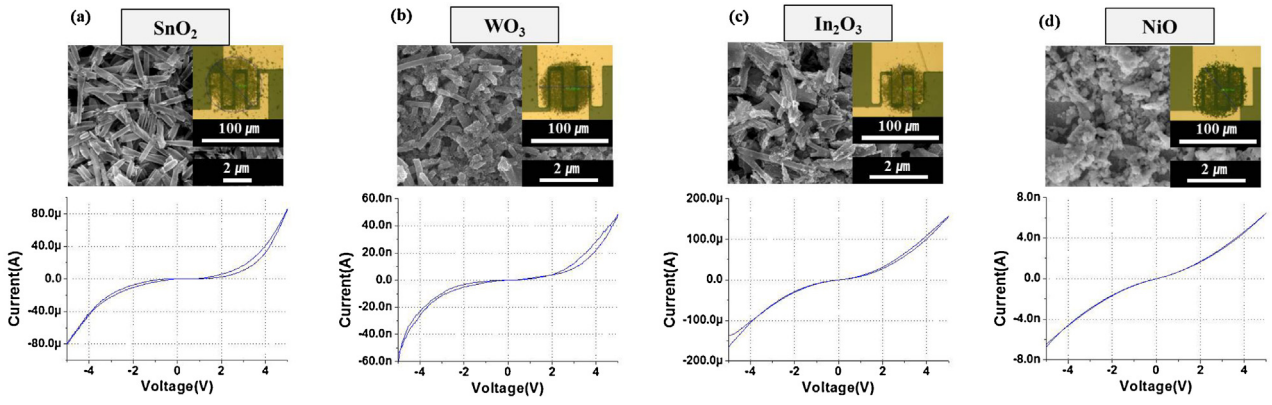

Fig. 6. Dot patterns of various electrospun metal oxide nanofibers on gold electrodes and their I–V characteristics: (a) SnO_2, (b) WO_3, (c) In_2O_3 and (d) NiO nanofiber patterns. Single jetting for each material is sufficient to form electrical connection between the sensing material and the electrodes.

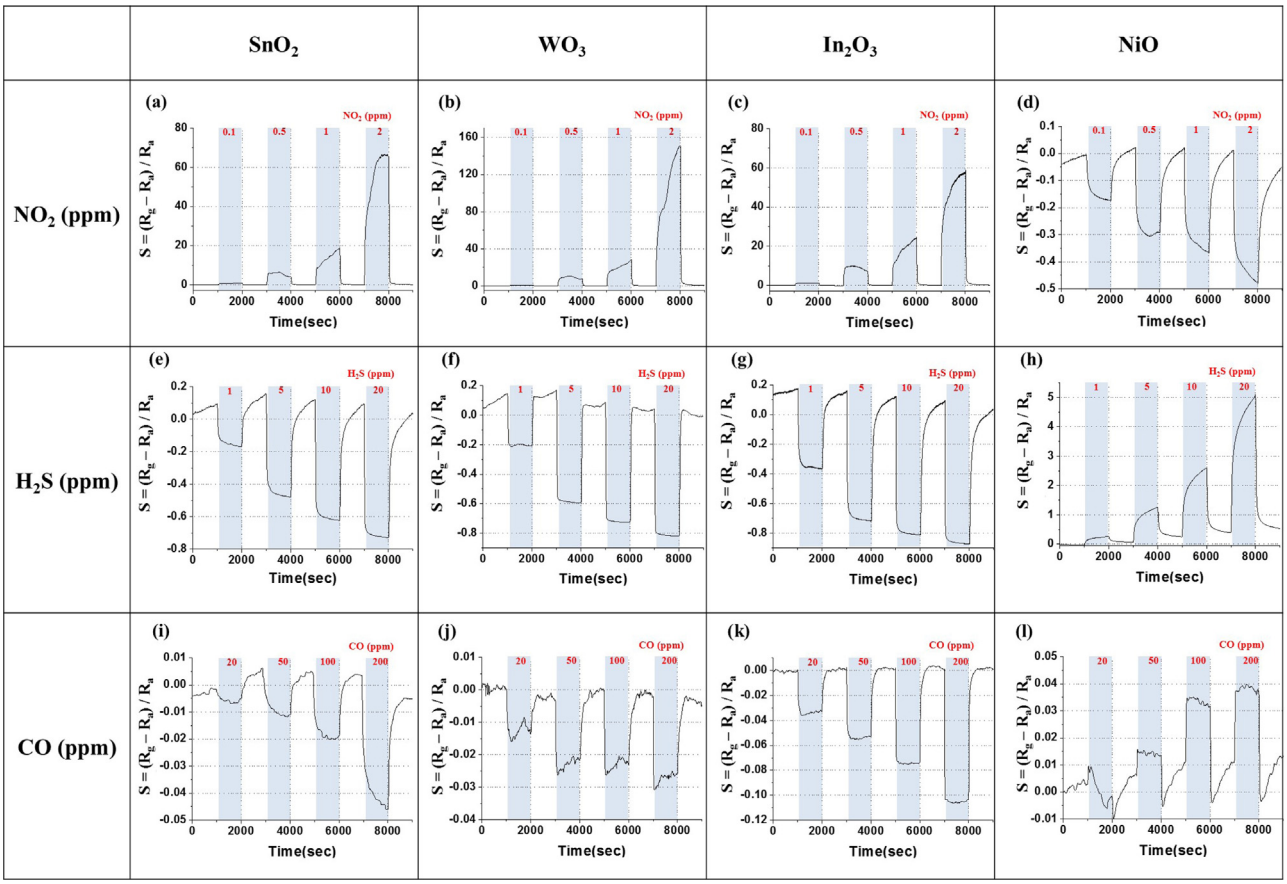

Fig. 7. Gas responses of EHD printed metal oxide gas sensors. Gas tests of SnO_2, WO_3, In_2O_3 and NiO nanofibers were conducted for NO_2, H_2S and CO gases at appropriate temperatures for each gas using a tube furnace. (a)–(d): NO_2 (0.1, 0.5, 1 and 2 ppm) at 300 °C, (e)–(h): H_2S (1, 5, 10 and 20 ppm) at 300 °C, (i)–(l): CO (20, 50, 100 and 200 ppm) at 450 °C. In the graph, Y axis represents the sensitivity ($S = (R_g - R_a)/R_a$).

At this bias, a cone shape meniscus was formed but monodisperse droplet was ejected from the apex of the meniscus in microdripping mode [38]. Individual droplet has smaller size than the pitch between droplets because the microdripping mode could just produce sequential dripping. Therefore, each droplet could not fill the space, thereby generating discontinuous line patterns. When the applied bias reaches the jetting mode voltage, continuous line pattern of 1D nanomaterial is generated.

Since the metal oxide gas sensors need high temperature for the operation, the area reduction of sensing materials is advantageous in order to lower the power needed to heat the sensing area. Towards this purpose, we utilized the EHD printing to fabricate highly compact gas sensor array of multiple gas sensing nanomaterials in microscale patterns, which is difficult by other patterning methods [24–27]. Pulsed waves consisting of base and jetting voltages were applied to the nozzle to generate microscale dot patterns of multiple types of nanomaterials.

Fig. 4 shows the dot patterns of various metal oxide nanofibers on the Au/SiO_2/Si substrate. The pattern sizes of electrospun nanofibers was smaller than the inner diameter (90 μm) of nozzle used for the EHD printing without clogging problem in the nozzle. The dot pattern sizes of SnO_2, WO_3, In_2O_3 and NiO nanofibers were 59.6 ± 4.7 μm, 43.3 ± 2.9 μm, 56.2 ± 4.8 μm, 61.8 ± 5.1 μm, which verifies that the fabrication of sub–60 μm sensing areas can be easily realized using EHD printing. When smaller nozzle was used and pulse width was optimized for EHD printing, sub–40 μm patterns could be achieved as shown in Fig. S5 (Supplementary Information). In case of smaller nozzle, electric field from the nozzle to the substrate is sharply focused and with this condition, it induces smaller droplets from the nozzle to the substrate [30]. Higher resolution SEM images reveal that the geometry of nanofiber fragments was well maintained after the EHD printing process (Fig. 4(e)–(h)).

By using the EHD printing process, the area of sensing materials can be easily controlled according to the abovementioned explanation. The statistical data in Fig. 5 presents the pattern sizes for different pulse widths. Printing experiment was conducted 6 times for each pulse width, and average pattern sizes and standard deviations were calculated. As a result, according to the increased pulse width (100 ms, 500 ms and 1 s), SnO_2 patterns exhibited 59.6 ± 4.7 μm, 70.7 ± 10.0 μm, 83.9 ± 11.1 μm in diameter, WO_3 patterns showed 43.3 ± 2.9 μm, 68.5 ± 5.6 μm, 79.8 ± 2.7 μm in diameter, In_2O_3 patterns had 56.2 ± 4.8 μm, 78.7 ± 6.7 μm, 90.2 ± 8.9 μm in diameter and NiO patterns presented 61.8 ± 5.1 μm, 95.7 ± 15.7 μm, 132.6 ± 14.9 μm in diameter, respectively. In summary, the pattern size can be reduced by using shorter pulse width. As the pulse width is increased, the volume of solution is increased or multiple droplets can occur [31,32], resulting in larger pattern size.

For the gas sensor application, metal oxide gas sensor was fabricated by EHD printing of metal oxide nanofibers on gold electrodes as shown in Fig. 6. In order to align the nozzle to the Au electrodes, dual cameras installed in the EHD printing system were utilized. With 100 ms of pulse width, single dot patterns of electrospun nanofibers were formed on the gold sensing electrode. The average pattern sizes for SnO_2, WO_3, In_2O_3 and NiO nanofibers were 72.8 μm, 61.4 μm, 69.3 μm, 65.5 μm, respectively, and all the patterns were formed in the sensing electrode areas. For the resistive type gas sensors, sensing materials should be electrically connected

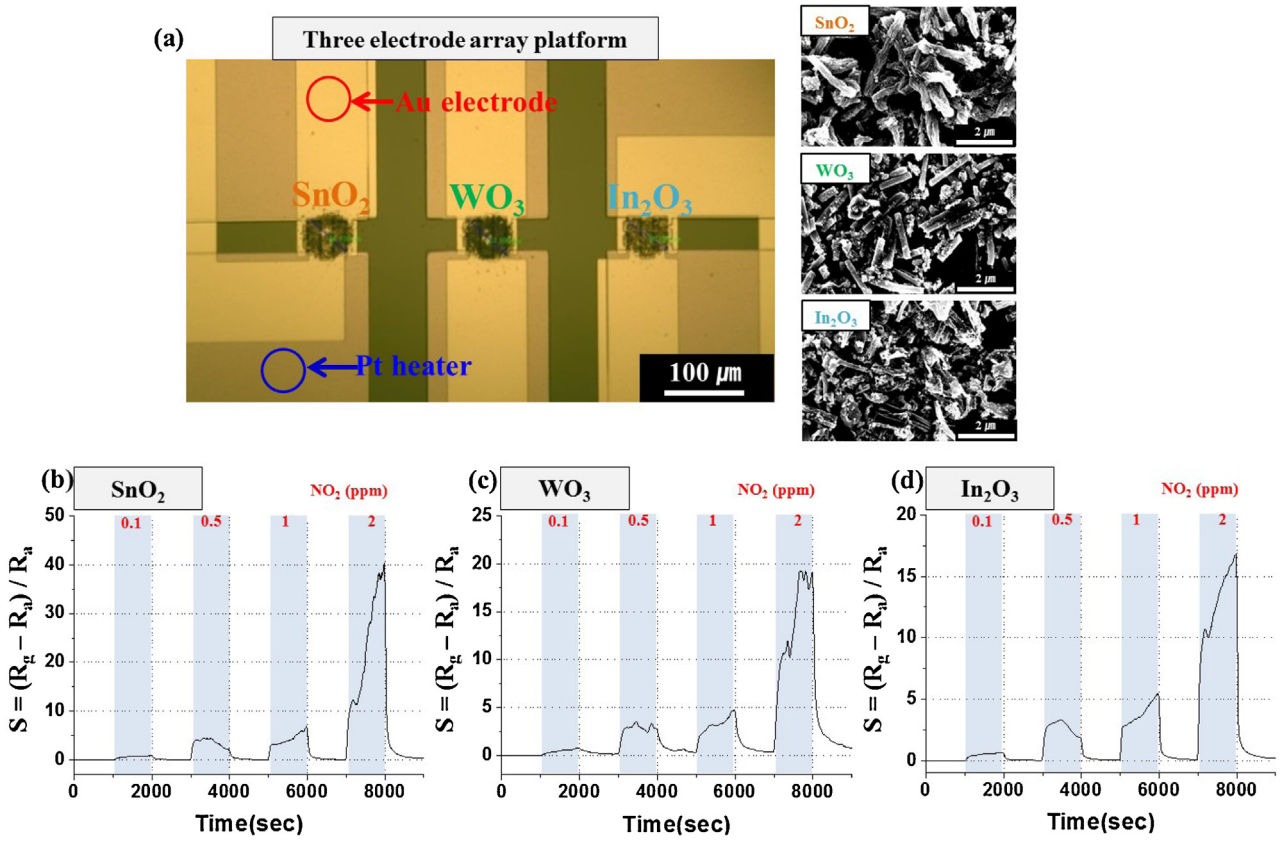

Fig. 8. (a) Gas sensor array of heterogeneous nanofibers fabricated by EHD printing on the Au sensing electrodes and Pt microheaters. (b–d) NO_2 gas sensing results of the sensor array: (b) SnO_2, (c) WO_3, (d) In_2O_3. Each material showed distinctive sensitivities at various gas concentrations.

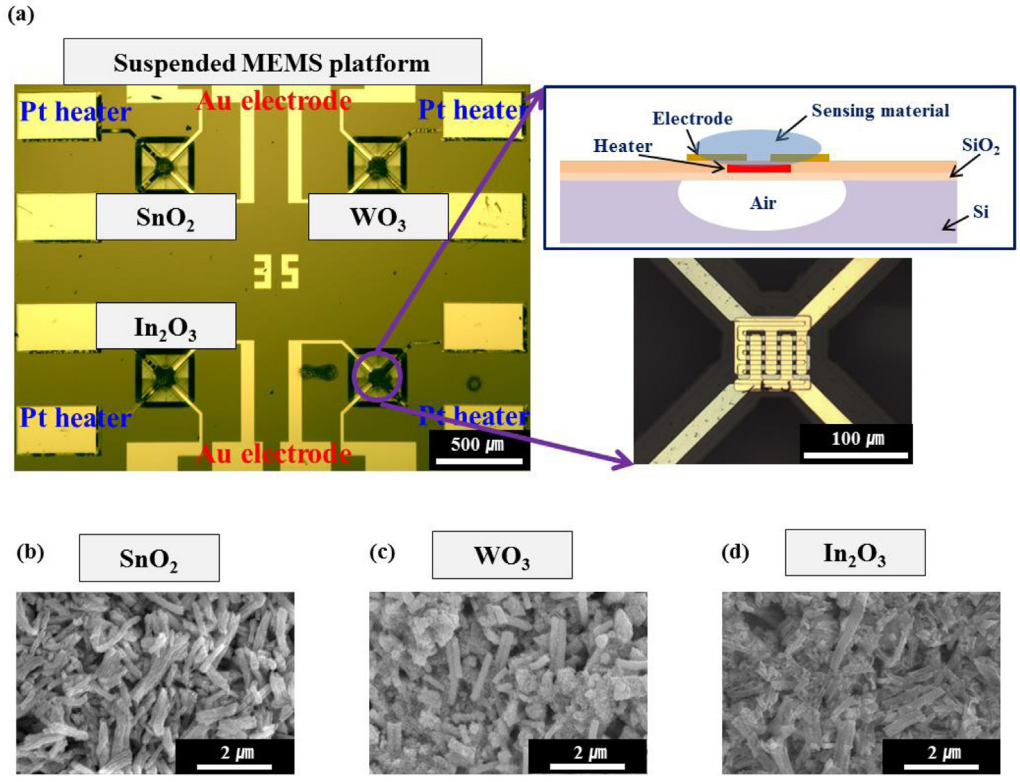

Fig. 9. (a) MEMS gas sensor array fabricated by EHD printing of SnO_2, WO_3 and In_2O_3 nanofibers for low power consumption. The platform size is 3.5 mm × 3.5 mm. (b–d) SEM image of nanofiber materials integrated on the suspended MEMS platform by EHD printing.

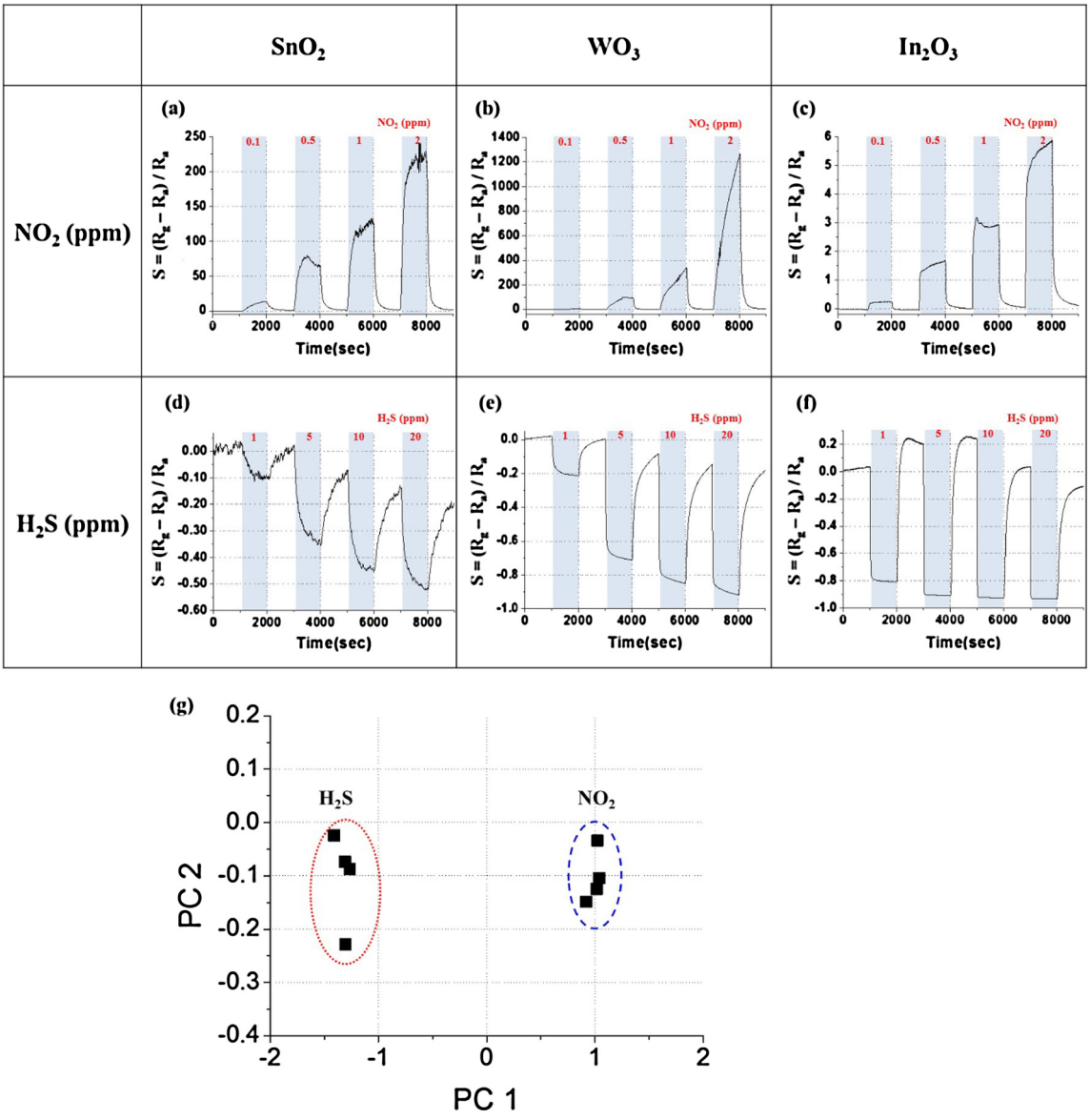

Fig. 10. (a-f) Sensing results of fabricated gas sensor array on MEMS platform. Gas tests of SnO_2, WO_3 and In_2O_3 nanofibers were conducted for NO_2 and H_2S gases with a power of 20 mW per microheater. (g) PCA results of EHD-printed SnO_2, WO_3 and In_2O_3 nanofiber gas sensor array for 0.1 ppm of NO_2 and 10 ppm of H_2S gases.

to the sensing electrode and continuous patterns should be formed to measure the resistance of sensing materials. If the inkjet printing is employed for the fabrication of resistive type gas sensor, repeated printing is required to form a continuous film with measureable electrical resistance [39,40]. On the contrary, in case of EHD printing, only single jetting is sufficient for the formation of continuous and conductive film patterns of the sensing material. This is because high concentration of sensing materials in the solution can be utilized without causing clogging problems in the nozzle if EHD printing is used. Fig. 6 shows the I–V characteristics of electrospun nanofibers patterned on the Au electrode by EHD printing, showing the formation of conductive films after single jetting.

Four kinds of metal oxide gas sensors (SnO_2, WO_3, In_2O_3, NiO) fabricated by EHD printing were used to test their responses to various target gases (NO_2, H_2S and CO) as shown in Fig. 7. For n-type metal oxides, oxygen molecules from the air get adsorbed on the surface of metal oxide and ionized to O_2-, O- by capturing electrons from the metal oxide in the atmospheric condition at 200–400 °C. This results in the formation of depletion region at the surface of metal oxide. In this case, upon the exposure to the oxidizing gas, oxygen molecule is adsorbed to the metal oxide surface working as electron acceptors, and the resistance is increased by expanding the depletion region [12,41,42]. On the other hand, reducing gases decrease the resistance of material by the reduction of depletion region via their reaction with surface adsorbed oxygen ions. Each gas sensing test was conducted in a tube furnace with an external heater to control the operational temperature of the gas sensor. For the gas response tests, each target gas was injected sequentially with synthesized air into the tube furnace containing the gas sensor. The operational temperature was set to optimize the gas sensitivities for each target gas (300 °C for NO_2 and H_2S, 450 °C for CO). All of metal oxide gas sensors were able to detect gases in the wide concentration ranges (i.e. 0.1–2 ppm for NO_2, 1–20 ppm for H_2S and 20–200 ppm for CO). Only NiO, which is a p-type semiconductor, showed opposite response directions than n-type semiconductors by the reaction with various target gases. The sensitivity of SnO_2, WO_3, In_2O_3 and NiO nanofiber sensors were approximately 60, 125, 55 and −0.45 for 2 ppm of NO_2 (sensitivity = $(R_g - R_a)/R_a$, R_a: resis-

tance in air and R_g: resistance in target gas). H_2S and CO, which are reducing gases, showed opposite resistance changes to the NO_2 in all the sensing materials as shown in Fig. 7(e–l).

The active area of each gas sensor is smaller than $100 \times 100\ \mu m^2$, and all sensors could detect NO_2 (0.1, 0.5, 1, and 2 ppm), H_2S (1, 5, 10, and 20 ppm) and CO (20, 50, 100, and 200 ppm) with different sensitivities at each concentration. WO_3 sensor has the highest sensitivity to 2 ppm of NO_2 and In_2O_3 sensor has a good sensing performance to various concentrations of H_2S. Although all the sensors showed low sensitivity to CO gas, In_2O_3 and NiO sensor exhibited better response and recovery speeds among them. SnO_2 and WO_3 sensors showed 229 s/273 s and 27 s/215 s (response time/recovery time), respectively. On the other hand, In_2O_3 and NiO showed more rapid response and recovery (response time/recovery time of 24 s/92 s and 32 s/43 s, respectively). Here, these values were defined as the time periods required to reach 90% of the total change during the gas injection/extraction cycles. Metal oxide gas sensor reacts with all kinds of gases but the sensitivity is different with each material. In general, surface modification or modulation of operating temperature can optimize sensitivity to specific gases [12,43]. These approaches will be employed to enhance the sensitivity and selectivity of the gas sensor array in the future.

An integrated gas sensor array with microheaters was fabricated by EHD printing of three different metal oxide nanofibers (Fig. 8(a)). Using the same EHD printing condition, SnO_2, WO_3 and In_2O_3 nanofiber solutions were printed sequentially on the sensor platform with three sets of sensing electrodes and microheaters. The nozzle and the sensor substrate were aligned using dual cameras and X-Y motion stage. As a result, an array of heterogeneous metal oxide nanofibers could be easily integrated in the active device area of $500 \times 100\ \mu m^2$. As shown in Fig. 8(b–d), sensing results were achieved by three sensing materials at the same time. All microheaters were operated at a bias of 4.5 V for NO_2 detection. The resistance of SnO_2, WO_3 and In_2O_3 was increased when NO_2 reacted with these materials. The sensitivities to 2 ppm of NO_2 gas were 35, 19 and 15 for SnO_2, WO_3 and In_2O_3 respectively. Since each sensing material has different sensitivity to individual target gases, it is possible to identify unknown gas or approximately determine individual gas concentration in a mixture gas by using principal component analysis (PCA) [44] or graphical analysis of multiple sensing data [9,44].

Finally, low power gas sensor array was fabricated by EHD printing of SnO_2, WO_3 and In_2O_3 nanofibers on a suspended MEMS microheater platform. As shown in Fig. 9, microscale patterns of these three materials could be well formed on an array of sensors without damaging the suspended MEMS bridge-plate structure. The SEM images in Fig. 9(b–d) reveals that the microstructures of short fragments of these nanofibers were well maintained. Fig. 10 shows the gas sensing performance of the fabricated sensor. For each microheater, 2.0–2.4 V was applied to consume approximately 20 mW of power. This power consumption is 32 times less than that needed for the substrate-bound microheater (~640 mW) because the suspended microheater is physically separated from the Si substrate and therefore conductive heat dissipation to the substrate is significantly reduced. SnO_2, WO_3 and In_2O_3 showed sensitivities of 210, 794 and 5.5 for 2 ppm of NO_2 and −0.48, −0.9 and −0.93 for 20 ppm of H_2S, respectively. WO_3 and In_2O_3 showed the best sensing performance for NO_2 for H_2S, respectively. The simultaneous sensing data from three metal oxide nanomaterials was used to identify the target gas by PCA method. Fig. 10(g) shows the results of plotting the responses of SnO_2, WO_3, and In_2O_3 nanofibers to NO_2 (0.1 ppm) and H_2S(10 ppm) with two principal components. As a result, two clusters were represented on a two-dimensional plane without overlapping with each other. This indicates that the sensor array of these three nanomaterials fabricated by EHD printing has the ability to distinguish between NO_2 and H_2S gases.

4. Conclusions

In conclusion, we demonstrated a microscale patterning process of electrospun metal oxide nanofibers for compact integrated gas sensor array by EHD printing method. Various microscale patterns of electrospun nanofibers could be successfully fabricated by EHD printing of nanofiber fragment solutions. By using this printing method, we could fabricate integrated gas sensor array of heterogeneous metal oxide nanofibers. Several sensing materials were successfully integrated on the MEMS microheater platform and low power multiplexed gas sensor was realized. As compared to conventional fabrication methods for metal oxide gas sensors such as screen printing, sputtering and drop casting, EHD printing method is much simpler without requirement of vacuum deposition or screen mask. Additionally, EHD printing method can generate fine patterns of dense gas sensing nanomaterials well below 100 μm by single jet, differently from the inkjet printing. This printing method would be very useful to fabricate a low power, compact and multiplexed gas sensor array towards internet of things (IoT) applications such as personalized air quality or health monitoring.

Acknowledgements

This work was supported by the National Research Foundation of Korea (NRF) Grant funded by the Korean Government (MSIP) (No. 2015R1A5A1037668).

Appendix A. Supplementary data

Supplementary data associated with this article can be found, in the online version, at http://dx.doi.org/10.1016/j.snb.2017.04.194.

References

[1] Y. Wang, M.M. Tong, D. Zhang, Z. Gao, Improving the performance of catalytic combustion type methane gas sensors using nanostructure elements doped with rare Earth cocatalysts, Sensors 11 (2011) 19–31.
[2] T. Hyodo, C. Ishibashi, K. Matsuo, K. Kaneyasu, H. Yanagi, Y. Shimizu, CO and CO2 sensing properties of electrochemical gas sensors using an anion-conducting polymer as an electrolyte, Electrochim. Acta 82 (2012) 19–25.
[3] G. Lu, N. Miura, N. Yamazoe, Stabilized zirconia-based sensors using WO3 electrode for detection of NO or NO2, Sens. Actuators B 65 (2000) 125–127.
[4] J.H. Ahn, J. Yun, D.I. Moon, Y.K. Choi, I. Park, Self-heated silicon nanowires for high performance hydrogen gas detection, Nanotechnology 26 (2015) 095501.
[5] J.H. Ahn, J. Yun, Y.K. Choi, I. Park, Palladium nanoparticle decorated silicon nanowire field-effect transistor with side-gates for hydrogen gas detection, Appl. Phys. Lett. 104 (2014).
[6] B. Choi, J.H. Ahn, J. Lee, J. Yoon, J. Lee, M. Jeon, et al., A bottom-gate silicon nanowire field-effect transistor with functionalized palladium nanoparticles for hydrogen gas sensors, Solid State Electron. 114 (2015) 76–79.
[7] G. Korotcenkov, Metal oxides for solid-state gas sensors: what determines our choice? Mater. Sci. Eng.: B 139 (2007) 1–23.
[8] M.A. Lim, D.H. Kim, C.O. Park, Y.W. Lee, S.W. Han, Z.Y. Li, et al., A new route toward ultrasensitive, flexible chemical sensors: metal nanotubes by wet-chemical synthesis along sacrificial nanowire templates, ACS Nano 6 (2012) 598–608.
[9] D. Yang, M.K. Fuadi, K. Kang, D. Kim, Z. Li, I. Park, Multiplexed gas sensor based on heterogeneous metal oxide nanomaterial array enabled by localized liquid-phase reaction, ACS Appl. Mater. Interfaces 7 (2015) 10152–10161.
[10] D. Yang, K. Kang, D. Kim, Z. Li, I. Park, Fabrication of heterogeneous nanomaterial array by programmable heating and chemical supply within microfluidic platform towards multiplexed gas sensing application, Sci. Rep. 5 (2015) 8149.
[11] D. Yang, D. Kim, S.H. Ko, A.P. Pisano, Z.Y. Li, I. Park, Focused energy field method for the localized synthesis and direct integration of 1D nanomaterials on microelectronic devices, Adv. Mater. 27 (2015) 1207–1215.
[12] C.X. Wang, L.W. Yin, L.Y. Zhang, D. Xiang, R. Gao, Metal oxide gas sensors: sensitivity and influencing factors, Sensors 10 (2010) 2088–2106.
[13] H. Bai, G. Shi, Gas sensors based on conducting polymers, Sensors (Basel, Switzerland) 7 (2007) 267–307.

[14] Y.H. Kim, S.J. Kim, Y.J. Kim, Y.S. Shim, S.Y. Kim, B.H. Hong, et al., Self-activated transparent all-graphene gas sensor with endurance to humidity and mechanical bending, ACS Nano 9 (2015) 10453–10460.
[15] L.Q. Nguyen, P.Q. Phan, H.N. Duong, C.D. Nguyen, L.H. Nguyen, Enhancement of NH3 gas sensitivity at room temperature by carbon nanotube-based sensor coated with Co nanoparticles, Sensors 13 (2013) 1754–1762.
[16] J. Yun, C.Y. Jin, J.H. Ahn, S. Jeon, I. Park, A self-heated silicon nanowire array: selective surface modification with catalytic nanoparticles by nanoscale Joule heating and its gas sensing applications, Nanoscale 5 (2013) 6851–6856.
[17] S. Mousavi, K. Kang, J. Park, I. Park, A room temperature hydrogen sulfide gas sensor based on electrospun polyaniline-polyethylene oxide nanofibers directly written on flexible substrates, RSC Adv. 6 (2016) 104131–104138.
[18] B. Choi, D. Lee, J.H. Ahn, J. Yoon, J. Lee, M. Jeon, et al., Investigation of optimal hydrogen sensing performance in semiconducting carbon nanotube network transistors with palladium electrodes, Appl. Phys. Lett. 107 (2015).
[19] M. Stankova, P. Ivanov, E. Llobet, J. Brezmes, X. Vilanova, I. Gràcia, et al., Sputtered and screen-printed metal oxide-based integrated micro-sensor arrays for the quantitative analysis of gas mixtures, Sens. Actuators B 103 (2004) 23–30.
[20] W.M. Sears, K. Colbow, R. Slamka, F. Consadori, Selective thermally cycled gas sensing using fast Fourier-transform techniques, Sens. Actuators B 2 (1990) 283–289.
[21] B.-J. Kim, J.-S. Kim, Gas sensing characteristics of MEMS gas sensor arrays in binary mixed-gas system, Mater. Chem. Phys. 138 (2013) 366–374.
[22] A.A. Tomchenko, G.P. Harmer, B.T. Marquis, J.W. Allen, Semiconducting metal oxide sensor array for the selective detection of combustion gases, Sens. Actuators B 93 (2003) 126–134.
[23] D. Kim, D. Yang, K. Kang, M.A. Lim, Z.Y. Li, C.O. Park, et al., In-situ integration and surface modification of functional nanomaterials by localized hydrothermal reaction for integrated and high performance chemical sensors, Sens. Actuators B–Chem. 226 (2016) 579–588.
[24] G. Sberveglieri, Classical and novel techniques for the preparation of SnO2 thin-film gas sensors, Sens. Actuators B 6 (1992) 239–247.
[25] J. Puigcorbé, A. Vilà, J. Cerdà, A. Cirera, I. Gràcia, C. Cané, et al., Thermo-mechanical analysis of micro-drop coated gas sensors, Sens. Actuators A: Phys. 97–98 (2002) 379–385.
[26] R.E. Cavicchi, R.M. Walton, M. Aquino-Class, J.D. Allen, B. Panchapakesan, Spin-on nanoparticle tin oxide for microhotplate gas sensors, Sens. Actuators B 77 (2001) 145–154.
[27] C. Xie, L. Xiao, M. Hu, Z. Bai, X. Xia, D. Zeng, Fabrication and formaldehyde gas-sensing property of ZnO–MnO2 coplanar gas sensor arrays, Sens. Actuators B 145 (2010) 457–463.
[28] Z. Yin, Y. Huang, N. Bu, X. Wang, Y. Xiong, Inkjet printing for flexible electronics: materials, processes and equipments, Chin. Sci. Bull. 55 (2010) 3383–3407.
[29] S. Roy, Fabrication of micro- and nano-structured materials using mask-less processes, J. Phys. D: Appl. Phys. 40 (2007) R413–R426.
[30] J.U. Park, M. Hardy, S.J. Kang, K. Barton, K. Adair, D.K. Mukhopadhyay, et al., High-resolution electrohydrodynamic jet printing, Nat. Mater. 6 (2007) 782–789.
[31] F.D. Prasetyo, H.T. Yudistira, V.D. Nguyen, D. Byun, Ag dot morphologies printed using electrohydrodynamic (EHD) jet printing based on a drop-on-demand (DOD) operation, J. Micromech. Microeng. 23 (2013) 095028.
[32] S. Mishra, K.L. Barton, A.G. Alleyne, P.M. Ferreira, J.A. Rogers, High-speed and drop-on-demand printing with a pulsed electrohydrodynamic jet, J. Micromech. Microeng. 20 (2010) 095026.
[33] N.G. Cho, D.J. Yang, M.-J. Jin, H.-G. Kim, H.L. Tuller, I.-D. Kim, Highly sensitive SnO2 hollow nanofiber-based NO2 gas sensors, Sens. Actuators B 160 (2011) 1468–1472.
[34] S.-H. Choi, G. Ankonina, D.-Y. Youn, S.-G. Oh, J.-M. Hong, A. Rothschild, et al., Hollow ZnO nanofibers fabricated using electrospun polymer templates and their electronic transport properties, ACS Nano 3 (2009) 2623–2631.
[35] D.-J. Yang, I. Kamienchick, D.Y. Youn, A. Rothschild, I.-D. Kim, Ultrasensitive and highly selective gas sensors based on electrospun SnO2 nanofibers modified by Pd loading, Adv. Funct. Mater. 20 (2010) 4258–4264.
[36] J. Shin, S.-J. Choi, I. Lee, D.-Y. Youn, C.O. Park, J.-H. Lee, et al., Thin-Wall assembled SnO2Fibers functionalized by catalytic Pt nanoparticles and their superior exhaled-Breath-Sensing properties for the diagnosis of diabetes, Adv. Funct. Mater. 23 (2013) 2357–2367.
[37] J.L. Li, On the meniscus deformation when the pulsed voltage is applied, J. Electrostat. 64 (2006) 44–52.
[38] J. Choi, Y.-J. Kim, S. Lee, S.U. Son, H.S. Ko, V.D. Nguyen, et al., Drop-on-demand printing of conductive ink by electrostatic field induced inkjet head, Appl. Phys. Lett. 93 (2008) 193508.
[39] B. Li, S. Santhanam, L. Schultz, M. Jeffries-El, M.C. Iovu, G. Sauvé, et al., Inkjet printed chemical sensor array based on polythiophene conductive polymers, Sens. Actuators B 123 (2007) 651–660.
[40] J. Kukkola, M. Mohl, A.-R. Leino, G. Tóth, M.-C. Wu, A. Shchukarev, et al., Inkjet-printed gas sensors: metal decorated WO3 nanoparticles and their gas sensing properties, J. Mater. Chem. 22 (2012) 17878.
[41] J.F. Mcaleer, P.T. Moseley, J.O.W. Norris, D.E. Williams, Tin dioxide gas sensors. 1. Aspects of the surface-chemistry revealed by electrical conductance variations, J. Chem. Soc. Faraday Trans. 1 (83) (1987) 1323–1346.
[42] G.F. Fine, L.M. Cavanagh, A. Afonja, R. Binions, Metal oxide semi-conductor gas sensors in environmental monitoring, Sensors 10 (2010) 5469–5502.
[43] M.M. Arafat, B. Dinan, S.A. Akbar, A.S. Haseeb, Gas sensors based on one dimensional nanostructured metal-oxides: a review, Sensors 12 (2012) 7207–7258.
[44] Y. Hu, H. Lee, S. Kim, M. Yun, A highly selective chemical sensor array based on nanowire/nanostructure for gas identification, Sens. Actuators B 181 (2013) 424–431.

Biographies

Kyungnam Kang received his B.S. in nanomechatronics engineering from Pusan National University (2013) and M.S. in mechanical engineering from KAIST (2015). He is currently a doctoral student at KAIST. His main research interests are nanomaterial-based sensors, MEMS fabrication and printing technologies.

Daejong Yang received his B.S. from Pusan National University (2009) and Ph.D. from KAIST (2014), both in mechanical engineering. He is currently a postdoctoral researcher at California Institute of Technology. His main research interests are hybrid nanofabrication, chemical sensors and nanophotonics-based sensors.

Jaeho Park received his B.S. from Hanyang University (2013) and M.S. from KAIST (2015), both in mechanical engineering. He is currently a doctoral student at KAIST. His main research interests are flexible micro physical/chemical sensor towards sensor integrated smart medical systems.

Sanghyeok Kim received his B.S. from Sogang University (2010), M.S. and Ph.D. from KAIST (2012, 2015), all in mechanical engineering. His main research interests are transfer printing and mechanical characterization of thin film.

Incheol Cho received his B.S. and M.S. from KAIST (2015, 2017), both in mechanical engineering. He is currently a doctoral student at KAIST. His main research interests are MEMS fabrication and highly integrated gas sensor based on nanomaterials.

Hyun-Ho Yang received his B.S., M.S., and Ph.D. from KAIST (2007, 2008, 2013), all in electrical engineering. He is currently a postdoctoral researcher at University of California, San Diego (UCSD). His main research interests are MEMS/NEMS actuators, RF MEMS devices and thermal MEMS/NEMS for THz imaging system.

Minkyu Cho received his B.S. from SUNY Buffalo (2009), M.S. and Ph.D. from University of Wisconsin-Madison (2011, 2015) all in electrical engineering. He is currently a postdoctoral researcher at KAIST. His main research interests are Si membrane device and low power gas sensors.

Saeb Mousavi received his B.S. from Iran University of Science and Technology (2012) and M.S. from KAIST (2016), both in mechanical engineering. His main research interests are ultra-low power/room temperature nano-gas sensors and wearable sensor platforms.

Kyung Hyun Choi received his B.S. and M.S. from Pusan National University and Ph.D. from University of Ottawa, all in mechanical engineering. He is currently a professor at the mechatronics engineering at Jeju National University. His main research interests are bio-inspired/bio-integrated electronics, solid state lighting and photovoltaics, semiconductors nanomaterials and carbon transistors.

Inkyu Park received his B.S., M.S., and Ph.D. from KAIST (1998), UIUC (2003) and UC Berkeley (2007), respectively, all in mechanical engineering. He has been with the department of mechanical engineering at KAIST since 2009 as a faculty and is currently an associate professor. His research interests are nanofabrication, smart sensors, nanomaterial-based sensors and flexible & wearable electronics. He has published more than 60 international journal articles (SCI indexed) and 100 international conference proceeding papers in the area of MEMS/NANO engineering. He is a recipient of IEEE NANO Best Paper Award (2010) and HP Open Innovation Research Award (2009–2012).